10.1071/CH13564_AC
©CSIRO 2014
Australian Journal of Chemistry 2014, 67(5), 701-710

SUPPLEMENTARY MATERIAL

Cobalt-mediated decarboxylative homocoupling of alkynyl carboxylic acids.

Michael G. Leeming,[a-c] George N. Khairallah,* [a-c] Sandra Osburn, [a-c]

Krista Vikse, [a-c] and Richard A. J. O'Hair* [a-c]

(a) School of Chemistry, University of Melbourne, Victoria 3010, Australia. Fax: 61 3 9347 5180; Tel: 61 3 8344 2452; E-mail: rohair@unimelb.edu.au

(b) Bio21 Institute of Molecular Science and Biotechnology, The University of Melbourne, Victoria 3010, Australia.

(c) ARC Centre of Excellence in Free Radical Chemistry and Biotechnology.

LIST OF FIGURES:

Figure S1: Decarboxylative Glaser-like C-C bond coupling via sequential CID of: (a) $CoCl(O_2CC{\equiv}CH)_2^-$ (*232 m/z*), (b) $CoCl(C{\equiv}CH)(O_2CC{\equiv}CH)^-$ (*188 m/z*), (c) $CoCl(C{\equiv}CH)_2^-$ (*144 m/z*), (d) $Co_2Cl_3(O_2CC{\equiv}CH)_2^-$ (*361 m/z*), (e) $Co_2Cl_3(C{\equiv}CH)(O_2CC{\equiv}CH)^-$ (*317 m/z*), (f) $Co_2Cl_3(C{\equiv}CH)_2^-$ (*273 m/z*).

Figure S2: Decarboxylative Glaser-like C-C bond coupling via sequential CID of: (a) $CoCl(O_2CC{\equiv}CCH_3)_2^-$ (*260 m/z*), (b) $CoCl(C{\equiv}CCH_3)(O_2CC{\equiv}CCH_3)^-$ (*216 m/z*), (c) $CoCl(C{\equiv}CCH_3)_2^-$ (*172 m/z*), (d) $Co_2Cl_3(O_2CC{\equiv}CCH_3)_2^-$ (*389 m/z*), (e) $Co_2Cl_3(C{\equiv}CCH_3)(O_2CC{\equiv}CCH_3)^-$ (*345 m/z*), (f) $Co_2Cl_3(C{\equiv}CCH_3)_2^-$ (*301 m/z*).

Figure S3: CID profile of the first decarboxylation of $Co_2Cl_3(O_2CC{\equiv}CPh)_2^-$.

Figure S4: CID profile of the second decarboxylation of $Co_2Cl_3(O_2CC{\equiv}CPh)_2^-$.

Figure S5: CID profile of the reductive elimination step of $Co_2Cl_3(O_2CC{\equiv}CPh)_2^-$.

Figure S6: CID profile of the first decarboxylation of $Co_2Cl_3(O_2CC{\equiv}CCH_3)_2^-$.

Figure S7: CID profile of the second decarboxylation of $Co_2Cl_3(O_2CC{\equiv}CCH_3)_2^-$.

Figure S8: CID profile of the reductive elimination step of $Co_2Cl_3(O_2CC{\equiv}CCH_3)_2^-$.

Figure S9: CID profile of the first decarboxylation of $Co_2Cl_3(O_2CC{\equiv}CH)_2^-$.

Figure S10: CID profile of the second decarboxylation of $Co_2Cl_3(O_2CC{\equiv}CH)_2^-$.

Figure S11: CID profile of the reductive elimination step of $Co_2Cl_3(O_2CC{\equiv}CH)_2^-$.

Figure S12: CID profile of the first decarboxylation of $CoCl(O_2CC{\equiv}CH)_2^-$.

Figure S13: CID profile of the second decarboxylation step of $CoCl(O_2CC{\equiv}CH)_2^-$.

Figure S14: CID profile of the reductive elimination step of $CoCl(O_2CC{\equiv}CH)_2^-$.

Figure S15: CID profile Comparison between bi- and mono-nuclear species of acetic acid for the first stage of CID.

Figure S16: CID profile of the first stage of CID of $Co_2Cl_3(O_2CCH_3)_2^-$.

Figure S17: CID profile of the first decarboxylation of $CoCl(O_2CCH_3)_2^-$.

Figure S18: CID profile of the radical anion formation of $CoCl(O_2CCH_3)_2^-$.

Figure S19: TOF mass spectrum of $Co_2Cl_3(O_2CC{\equiv}CPh)_2^-$ CID (513 *m/z*).

Figure S20: TOF mass spectrum of $Co_2Cl_3(O_2CC{\equiv}CPh)(C{\equiv}CPh)^-$ CID (469 *m/z*).

Figure S21: TOF mass spectrum of $Co_2Cl_3(C{\equiv}CPh)_2^-$ (425 *m/z*).

Figure S22: TOF mass spectrum of $Co_2Cl_3(O_2CC{\equiv}CCH_3)_2^-$ (389 *m/z*).

Figure S23: TOF mass spectrum of $Co_2Cl_3(C{\equiv}CCH_3)(O_2CC{\equiv}CCH_3)^-$ (347 *m/z*).

Figure S24: TOF mass spectrum of $Co_2Cl_3(C{\equiv}CCH_3)_2^-$ (301 *m/z*).

Figure S25: TOF mass spectrum of $Co_2Cl_3(O_2CC{\equiv}CH)_2^-$ (361 *m/z*).

Figure S26: TOF mass spectrum of $Co_2Cl_3(C{\equiv}CH)(O_2CC{\equiv}CH)^-$ (317 *m/z*).

Figure S27: TOF mass spectrum of $Co_2Cl_3(C{\equiv}CH)_2^-$ (273 *m/z*).

Figure S28: TOF mass spectrum of $CoCl(O_2CC{\equiv}CPh)_2^-$ (384 *m/z*).

Figure S29: TOF mass spectrum of $CoCl(C{\equiv}CPh)(O_2CC{\equiv}CPh)^-$ (340 *m/z*).

Figure S30: TOF mass spectrum of $CoCl(C{\equiv}CPh)_2^-$ (296 *m/z*).

Figure S31: TOF mass spectrum of $CoCl(O_2CC{\equiv}CCH_3)_2^-$ (260 *m/z*).

Figure S32: TOF mass spectrum of $CoCl(C{\equiv}CCH_3)(O_2CC{\equiv}CCH_3)^-$ (216 *m/z*).

Figure S33: TOF mass spectrum of $CoCl(C{\equiv}CCH_3)_2^-$ (172 *m/z*).

Figure S34: TOF mass spectrum of $CoCl(O_2CC{\equiv}CH)_2^-$ (232 *m/z*).

Figure S35: TOF mass spectrum of $CoCl(C{\equiv}CH)(O_2CC{\equiv}CH)^-$ (188 *m/z*).

Figure S36: TOF mass spectrum of $CoCl(C{\equiv}CH)_2^-$ (144 *m/z*).

Figure S1: Decarboxylative Glaser-like C-C bond coupling via sequential CID of: (a) $CoCl(O_2CC{\equiv}CH)_2^-$ (*232 m/z*), (b) $CoCl(C{\equiv}CH)(O_2CC{\equiv}CH)^-$ (*188 m/z*), (c) $CoCl(C{\equiv}CH)_2^-$ (*144 m/z*), (d) $Co_2Cl_3(O_2CC{\equiv}CH)_2^-$ (*361 m/z*), (e) $Co_2Cl_3(C{\equiv}CH)(O_2CC{\equiv}CH)^-$ (*317 m/z*), (f) $Co_2Cl_3(C{\equiv}CH)_2^-$ (*273 m/z*).

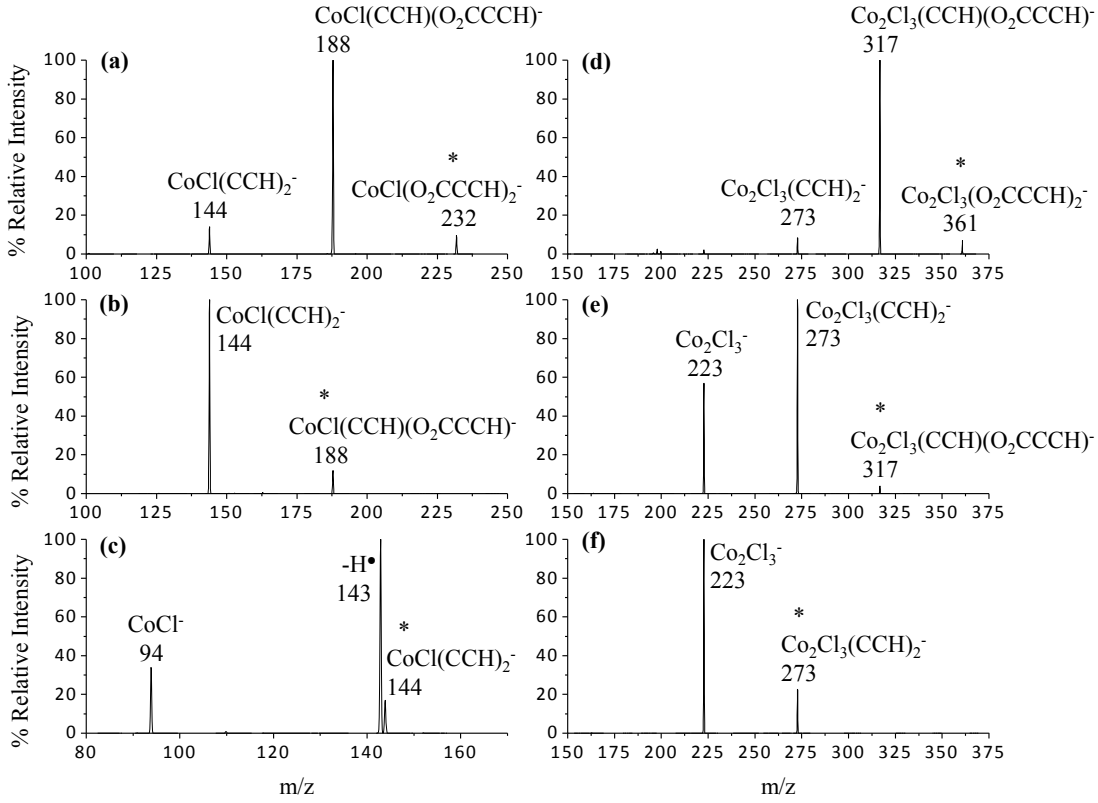

Figure S2: Decarboxylative Glaser-like C-C bond coupling via sequential CID of: (a) $CoCl(O_2CC{\equiv}CCH_3)_2^-$ (*260 m/z*), (b) $CoCl(C{\equiv}CCH_3)(O_2CC{\equiv}CCH_3)^-$ (*216 m/z*), (c) $CoCl(C{\equiv}CCH_3)_2^-$ (*172 m/z*), (d) $Co_2Cl_3(O_2CC{\equiv}CCH_3)_2^-$ (*389 m/z*), (e) $Co_2Cl_3(C{\equiv}CCH_3)(O_2CC{\equiv}CCH_3)^-$ (*345 m/z*), (f) $Co_2Cl_3(C{\equiv}CCH_3)_2^-$ (*301 m/z*).

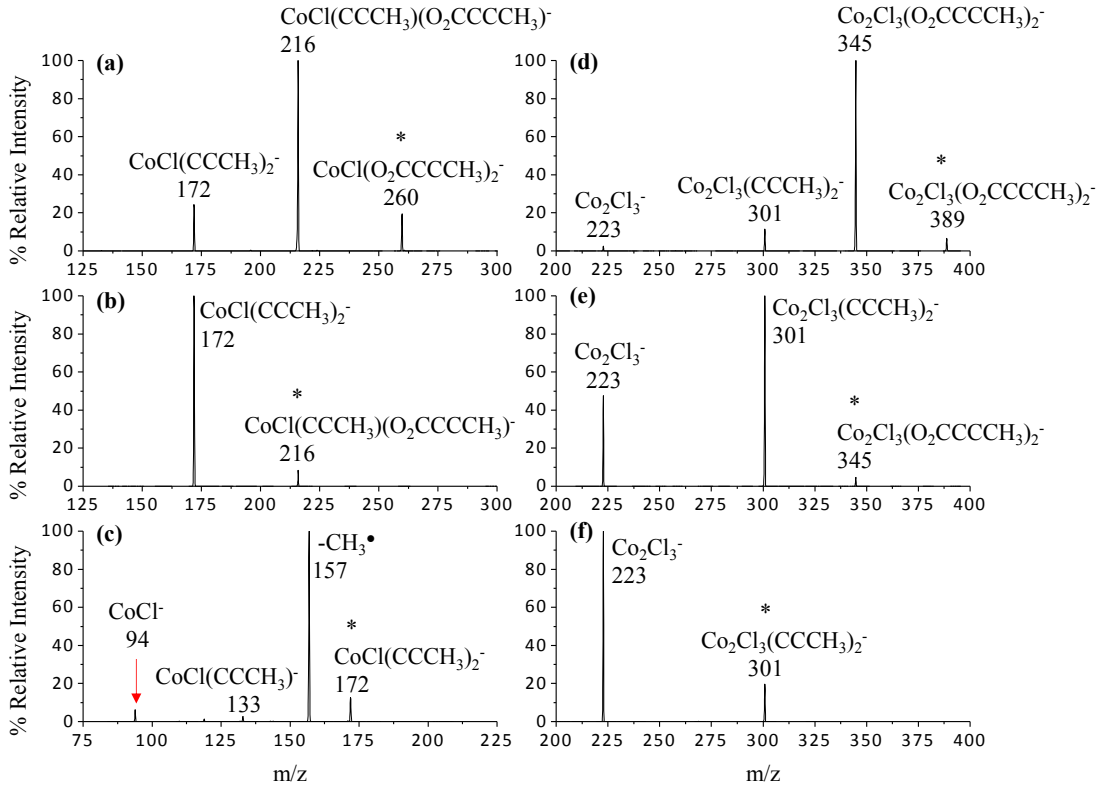

Figure S3: CID profile of the first decarboxylation of $Co_2Cl_3(O_2CC{\equiv}CPh)_2^-$.

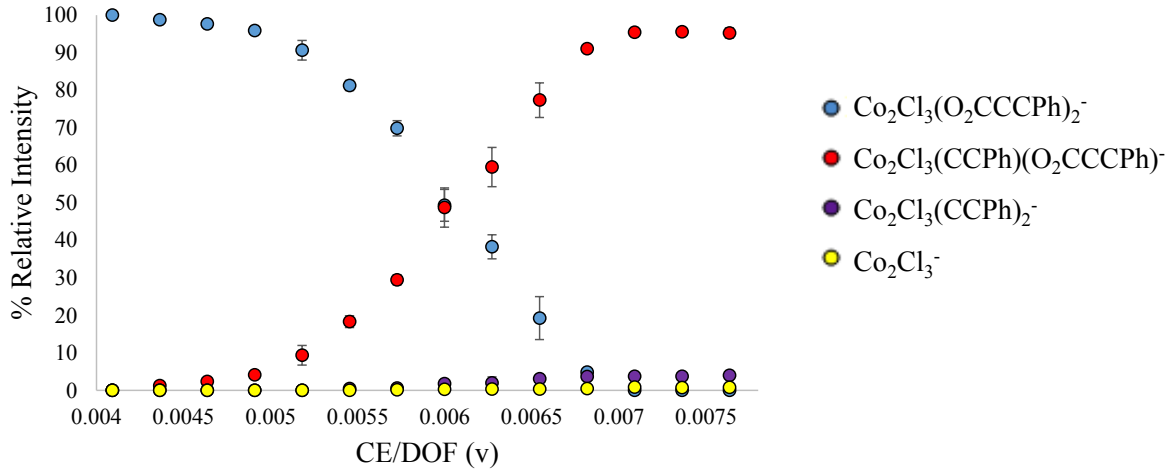

Figure S4: CID profile of the second decarboxylation of $Co_2Cl_3(O_2CC{\equiv}CPh)_2^-$.

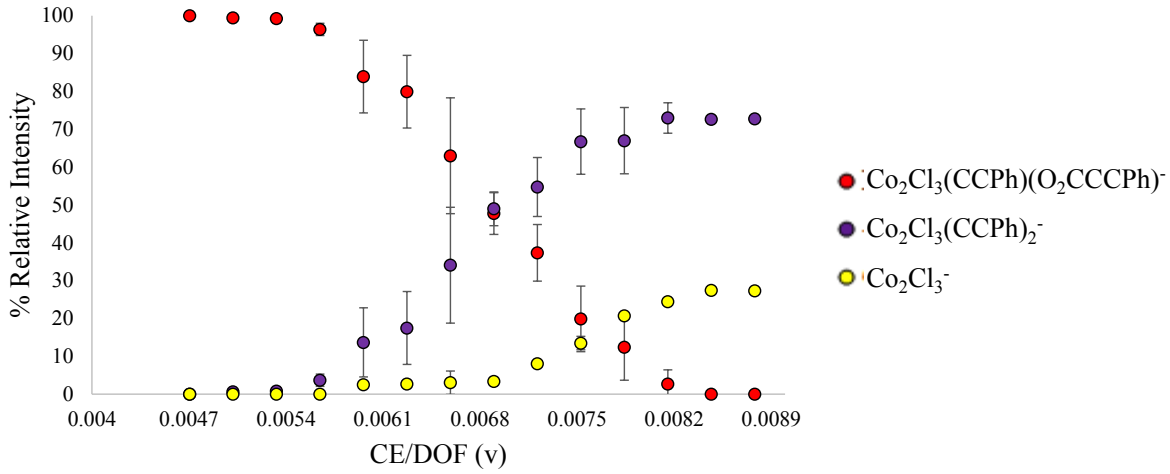

Figure S5: CID profile of the reductive elimination step of $Co_2Cl_3(O_2CC{\equiv}CPh)_2^-$.

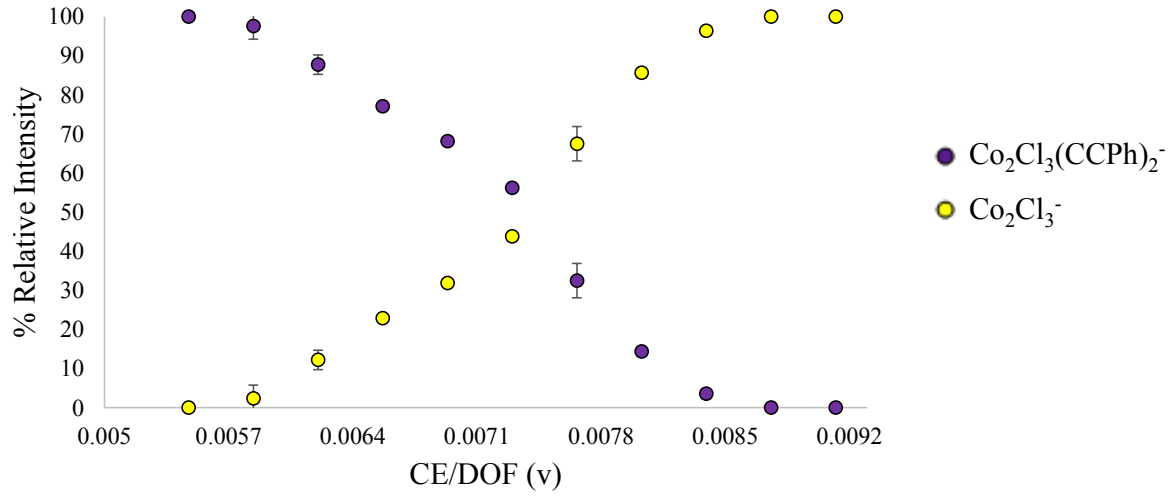

Figure S6: CID profile of the first decarboxylation of $Co_2Cl_3(O_2CC{\equiv}CCH_3)_2^-$.

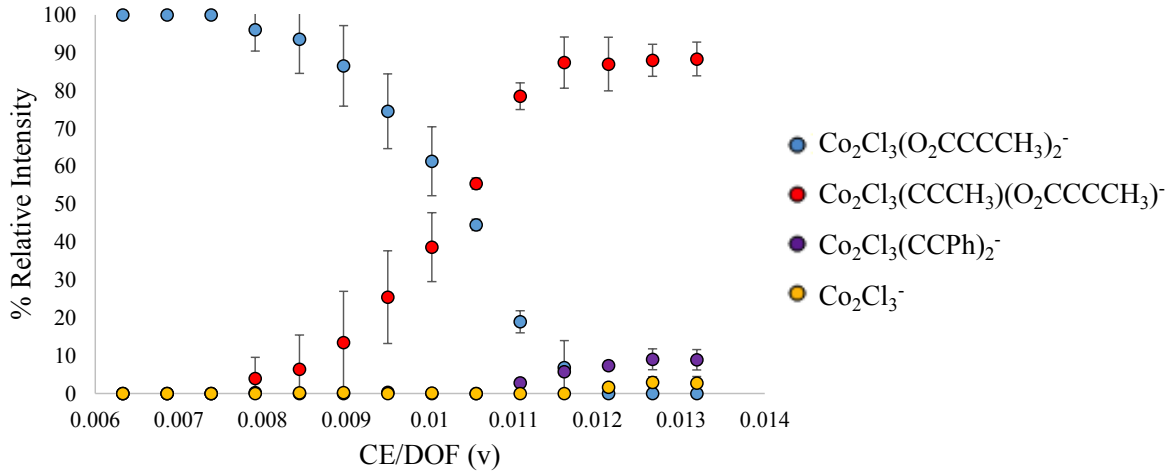

Figure S7: CID profile of the second decarboxylation of $Co_2Cl_3(O_2CC{\equiv}CCH_3)_2^-$.

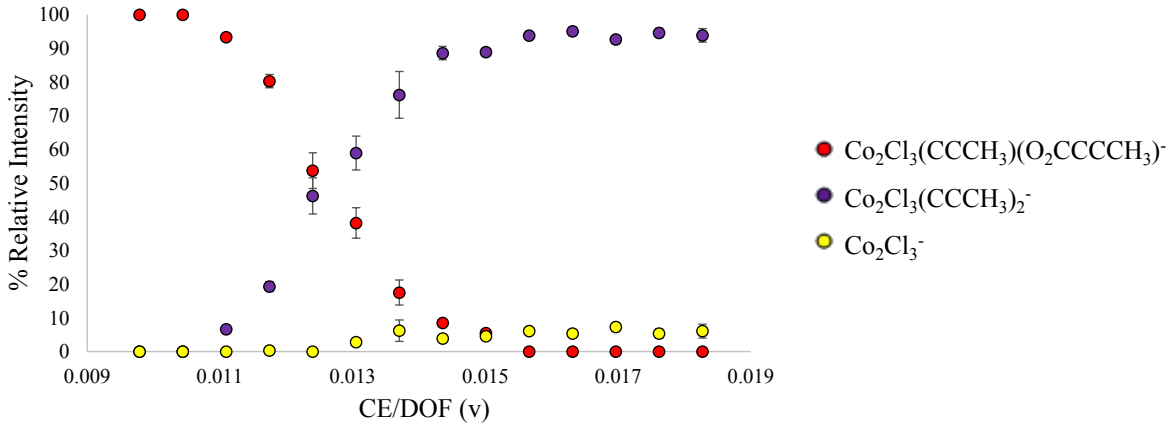

Figure S8: CID profile of the reductive elimination step of $Co_2Cl_3(O_2CC{\equiv}CCH_3)_2^-$.

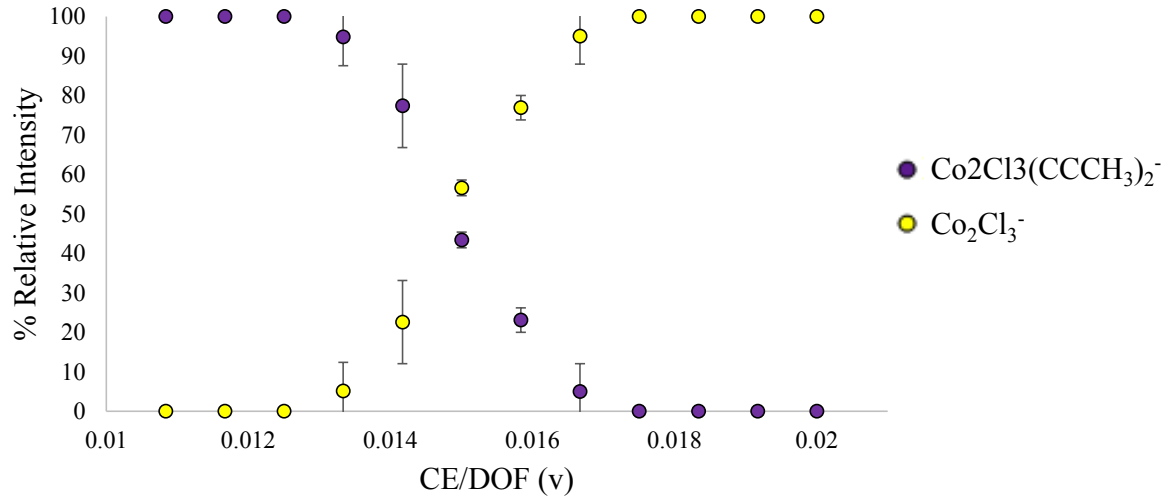

Figure S9: CID profile of the first decarboxylation of $Co_2Cl_3(O_2CC{\equiv}CH)_2^-$.

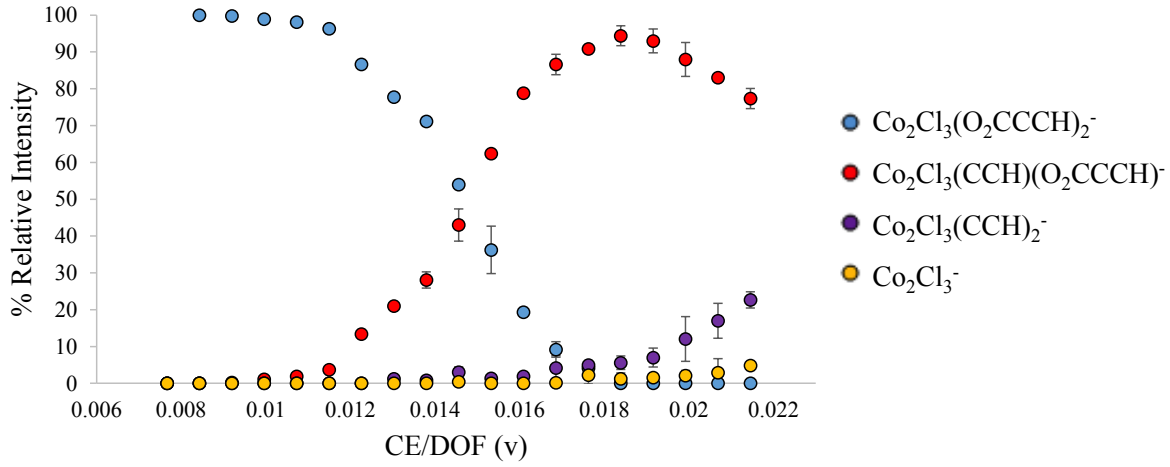

Figure S10: CID profile of the second decarboxylation of $Co_2Cl_3(O_2CC{\equiv}CH)_2^-$.

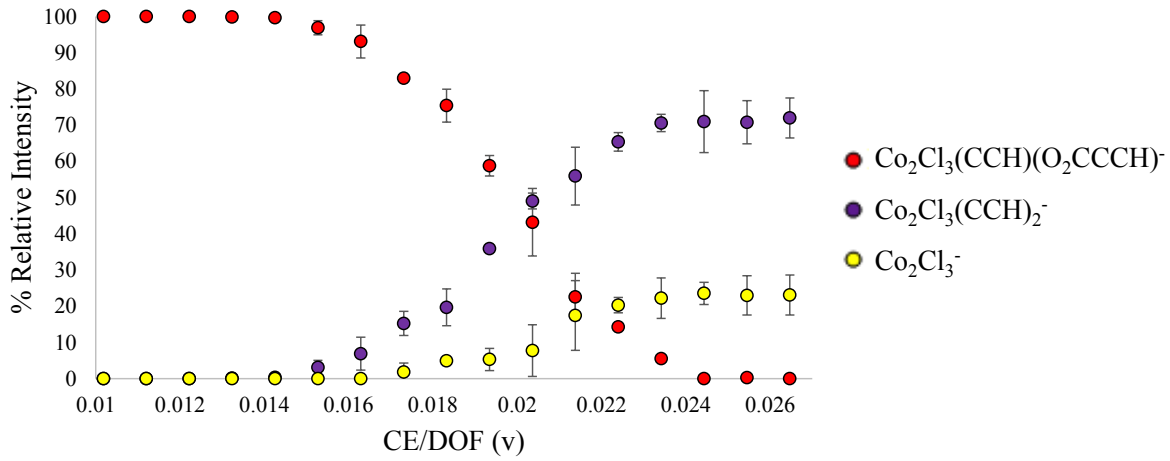

Figure S11: CID profile of the reductive elimination step of $Co_2Cl_3(O_2CC{\equiv}CH)_2^-$.

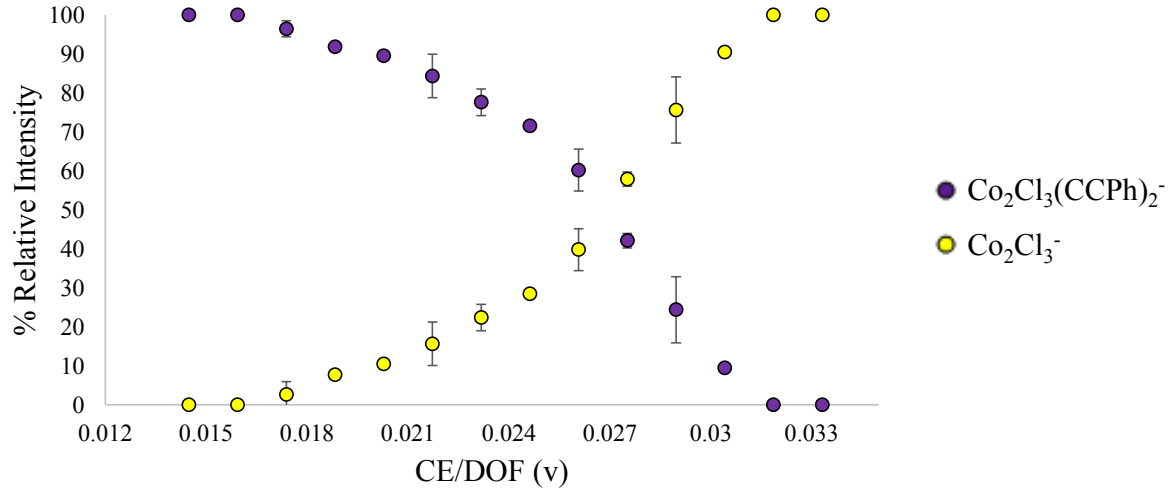

Figure S12: CID profile of the first decarboxylation of $CoCl(O_2CC{\equiv}CH)_2^-$.

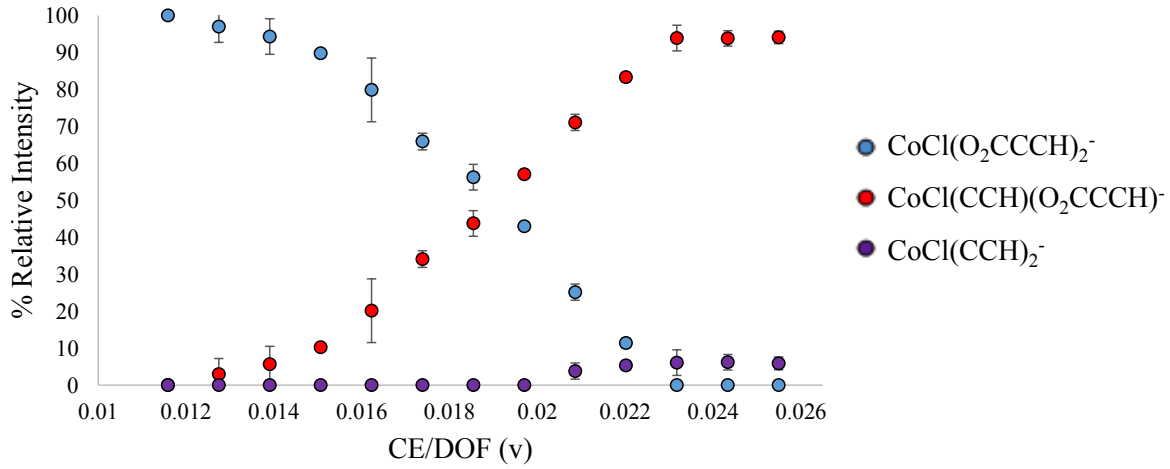

Figure S13: CID profile of the second decarboxylation step of $CoCl(O_2CC{\equiv}CH)_2^-$.

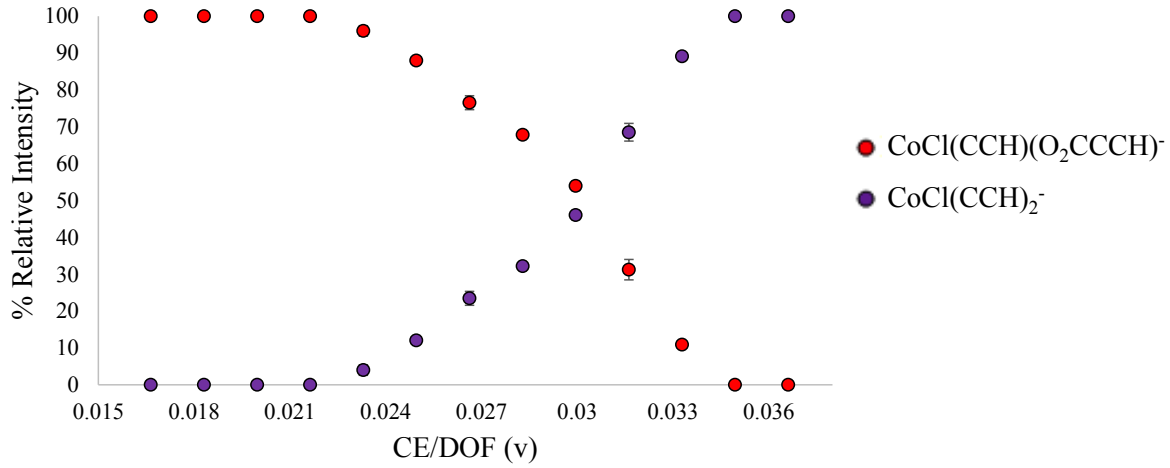

Figure S14: CID profile of the reductive elimination step of $CoCl(O_2CC{\equiv}CH)_2^-$.

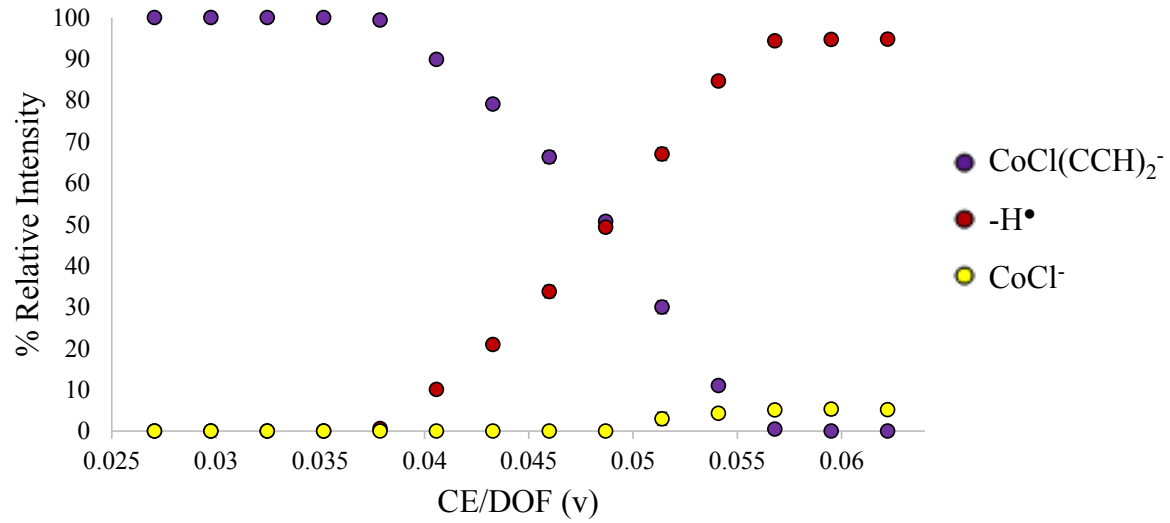

Figure S15: CID profile Comparison between bi- and mono-nuclear species of acetic acid for the first stage of CID.

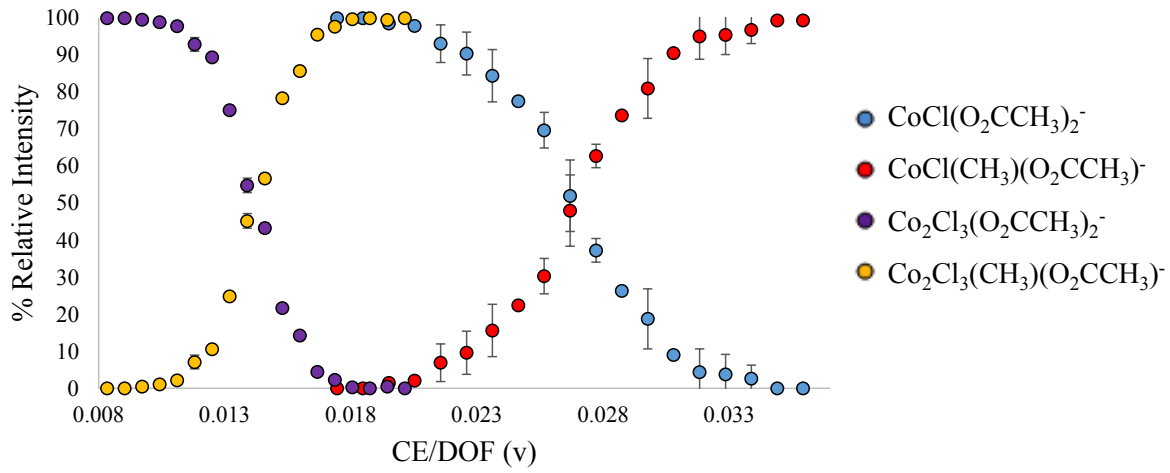

Figure S16: CID profile of the first stage of CID of $Co_2Cl_3(O_2CCH_3)_2^-$.

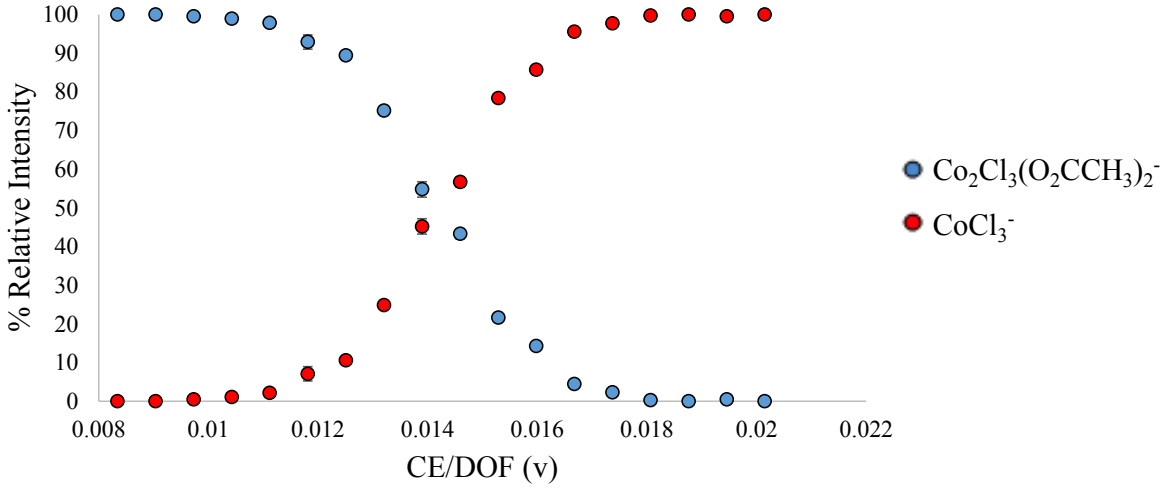

Figure S17: CID profile of the first decarboxylation of $CoCl(O_2CCH_3)_2^-$.

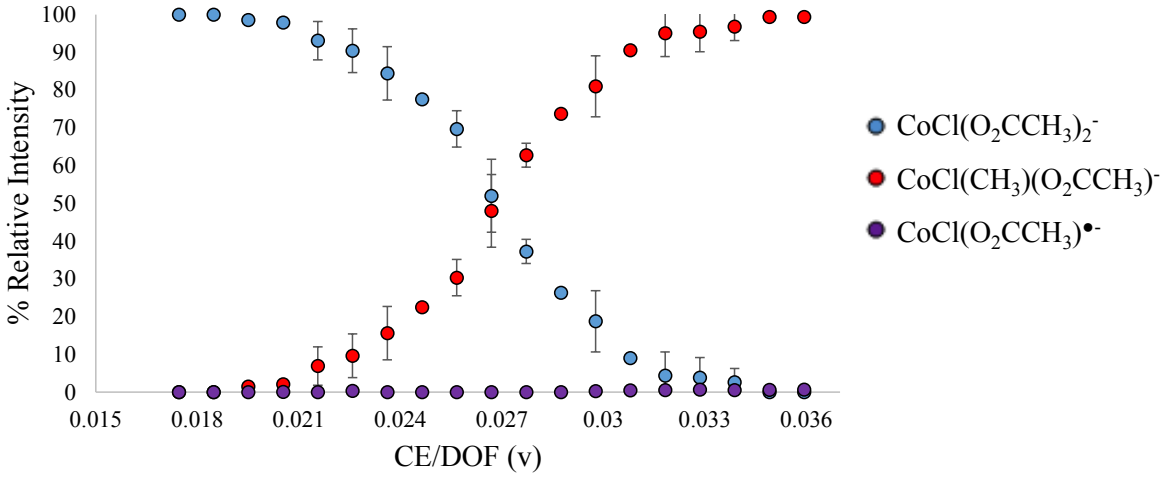

Figure S18: CID profile of the radical anion formation of $CoCl(O_2CCH_3)_2^-$.

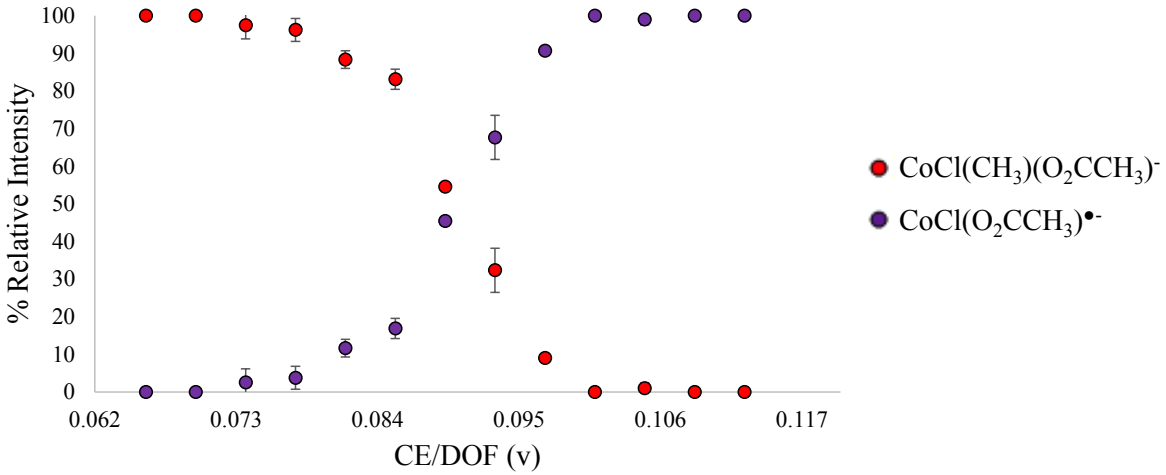

Figure S19: TOF mass spectrum of $Co_2Cl_3(O_2CC{\equiv}CPh)_2^-$ CID (513 *m/z*).

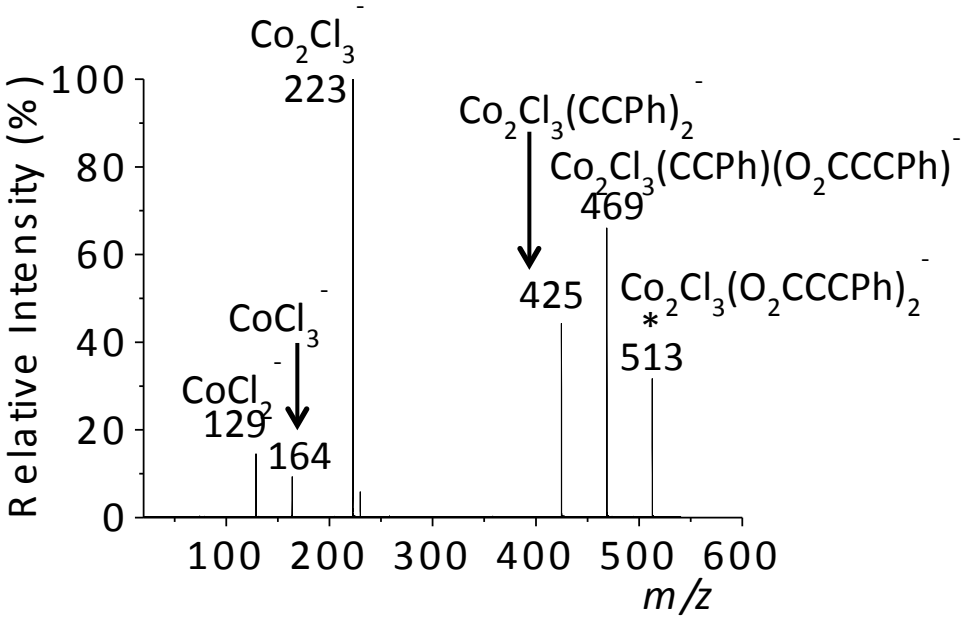

Figure S20: TOF mass spectrum of $Co_2Cl_3(O_2CC{\equiv}CPh)(C{\equiv}CPh)^-$ CID (469 *m/z*).

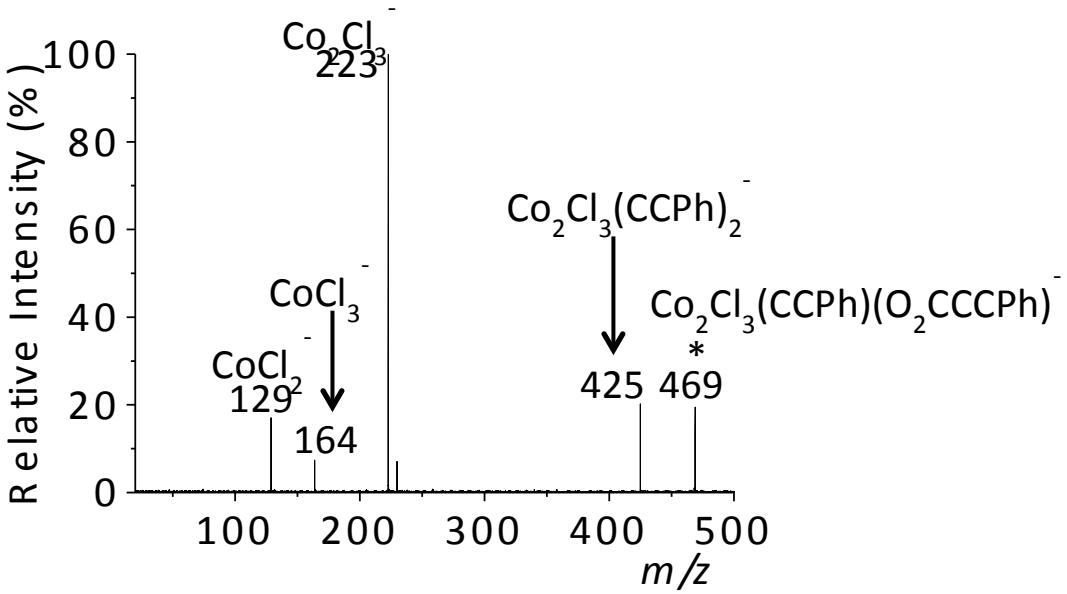

Figure S21: TOF mass spectrum of $Co_2Cl_3(C{\equiv}CPh)_2^-$ (425 *m/z*).

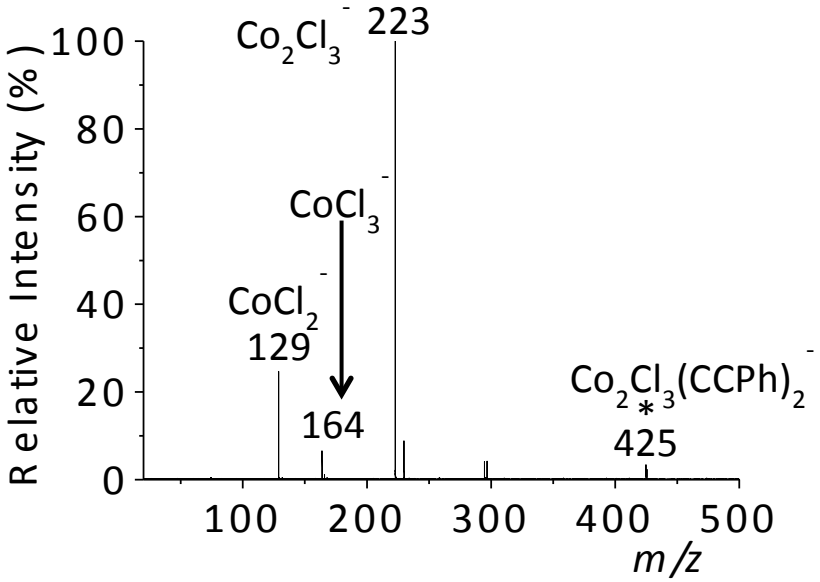

Figure S22: TOF mass spectrum of $Co_2Cl_3(O_2CC{\equiv}CCH_3)_2^-$ (389 *m/z*).

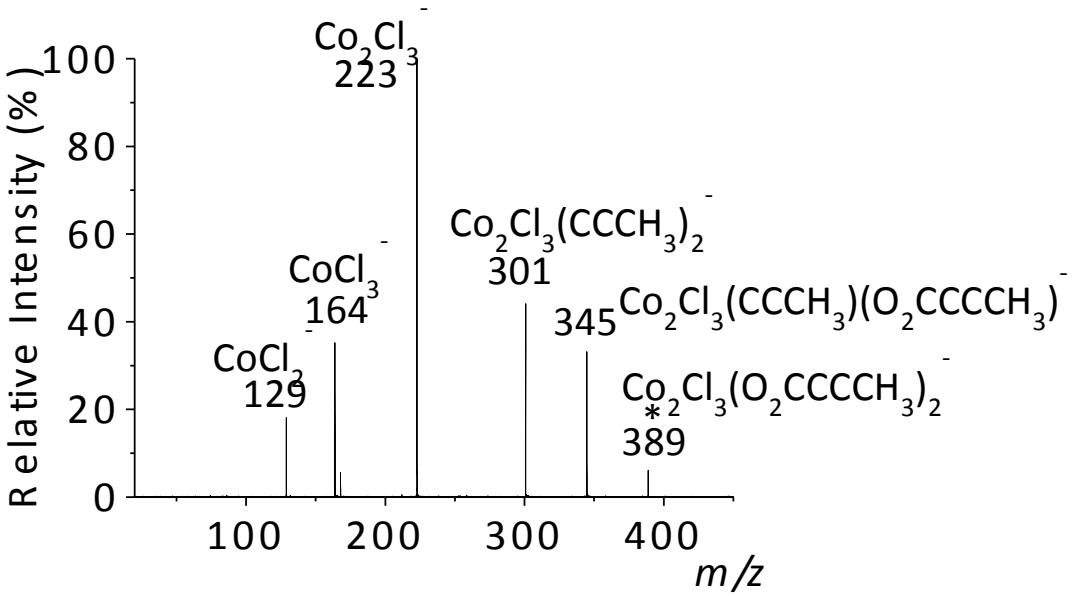

Figure S23: TOF mass spectrum of $Co_2Cl_3(C{\equiv}CCH_3)(O_2CC{\equiv}CCH_3)^-$ (347 *m/z*).

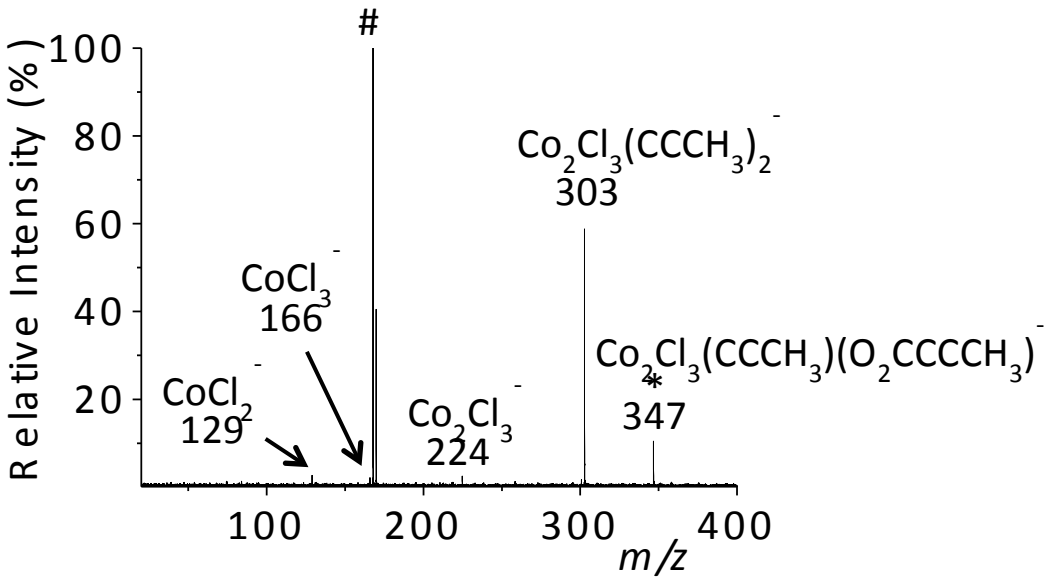

NB: Due to the presence of significant isobaric peaks in the MS1 spectrum, the A+2 ion has been isolated and subjected to CID in this case. The peak marked with # is assigned to the fragmentation product of an isobaric ion observed in the MS^1 spectrum.

Figure S24: TOF mass spectrum of $Co_2Cl_3(C{\equiv}CCH_3)_2^-$ (301 *m/z*).

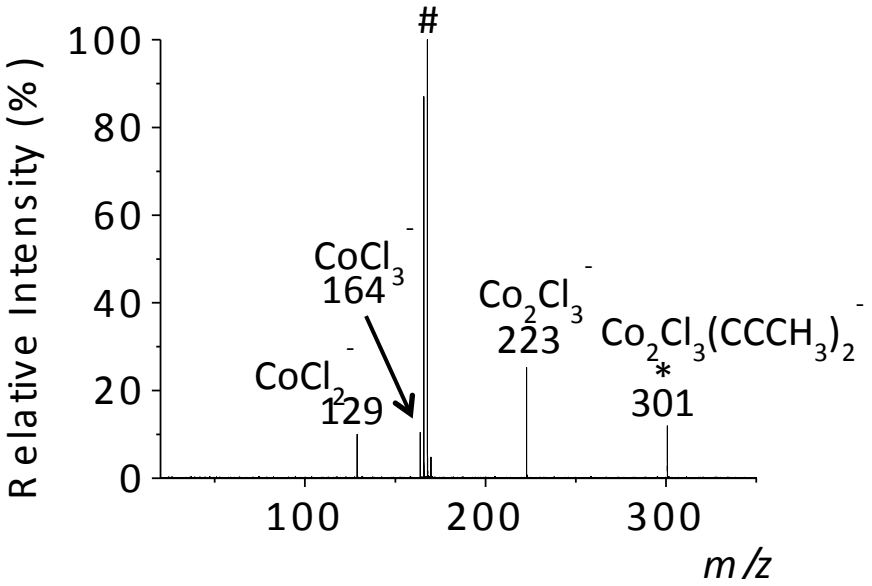

NB: Peak marked with # is assigned to the fragmentation product of an isobaric ion observed in the MS^1 spectrum

Figure S25: TOF mass spectrum of $Co_2Cl_3(O_2CC{\equiv}CH)_2^-$ (361 *m/z*).

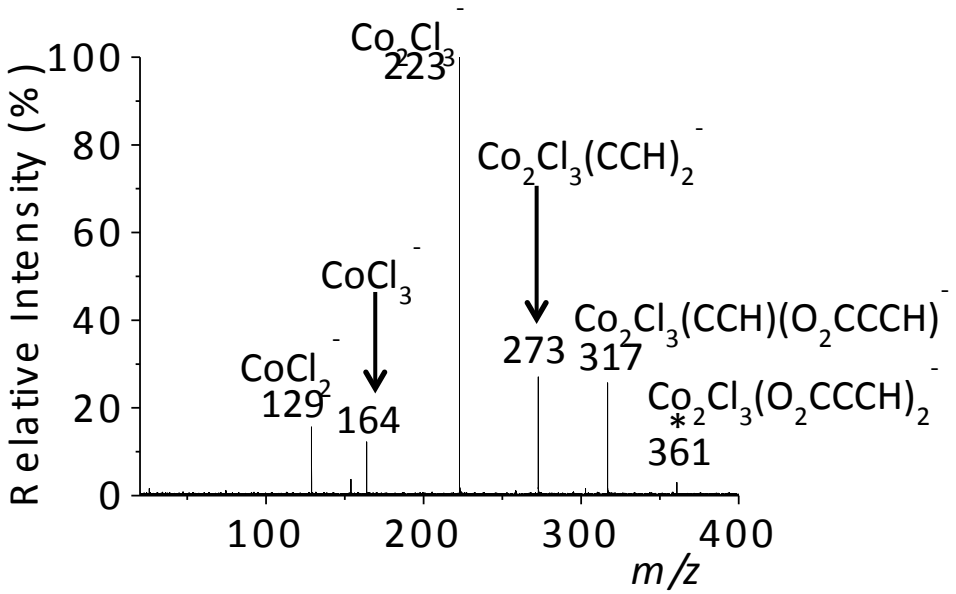

Figure S26: TOF mass spectrum of $Co_2Cl_3(C{\equiv}CH)(O_2CC{\equiv}CH)^-$ (317 *m/z*).

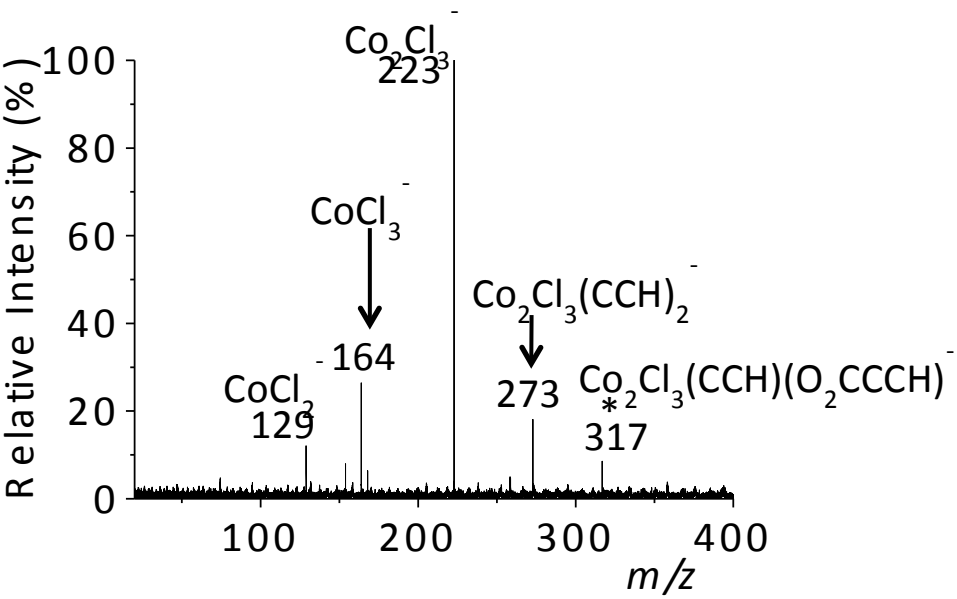

Figure S27: TOF mass spectrum of $Co_2Cl_3(C{\equiv}CH)_2^-$ (273 *m/z*).

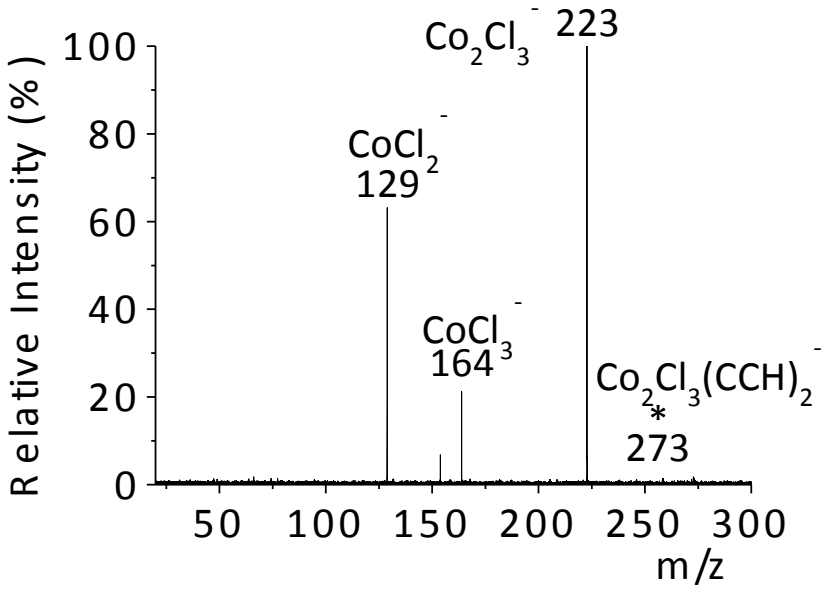

Figure S28: TOF mass spectrum of $CoCl(O_2CC{\equiv}CPh)_2^-$ (384 *m/z*).

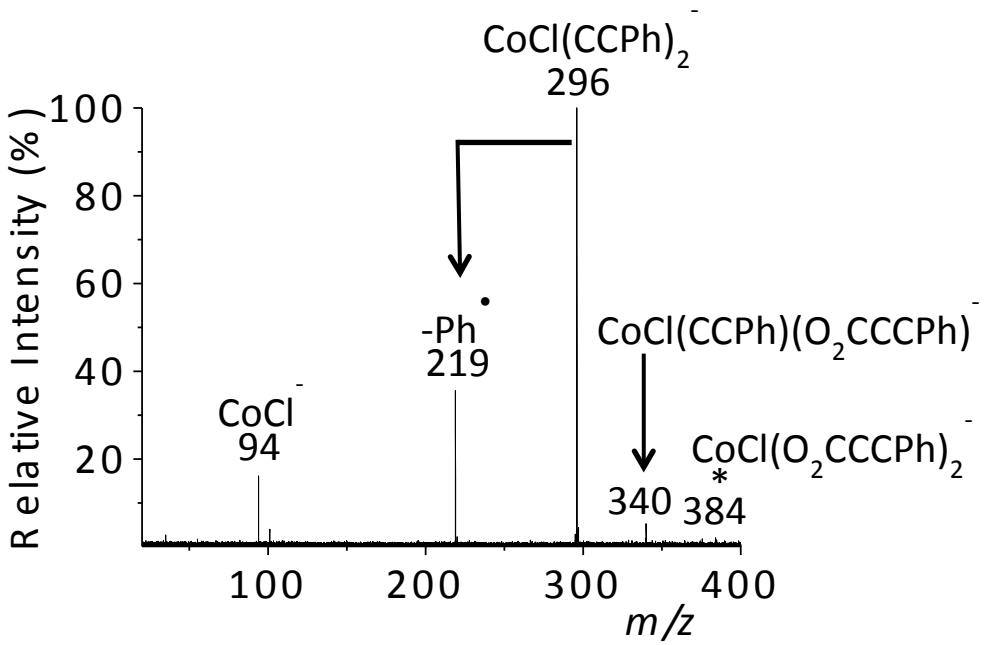

Figure S29: TOF mass spectrum of $CoCl(C{\equiv}CPh)(O_2CC{\equiv}CPh)^-$ (340 *m/z*).

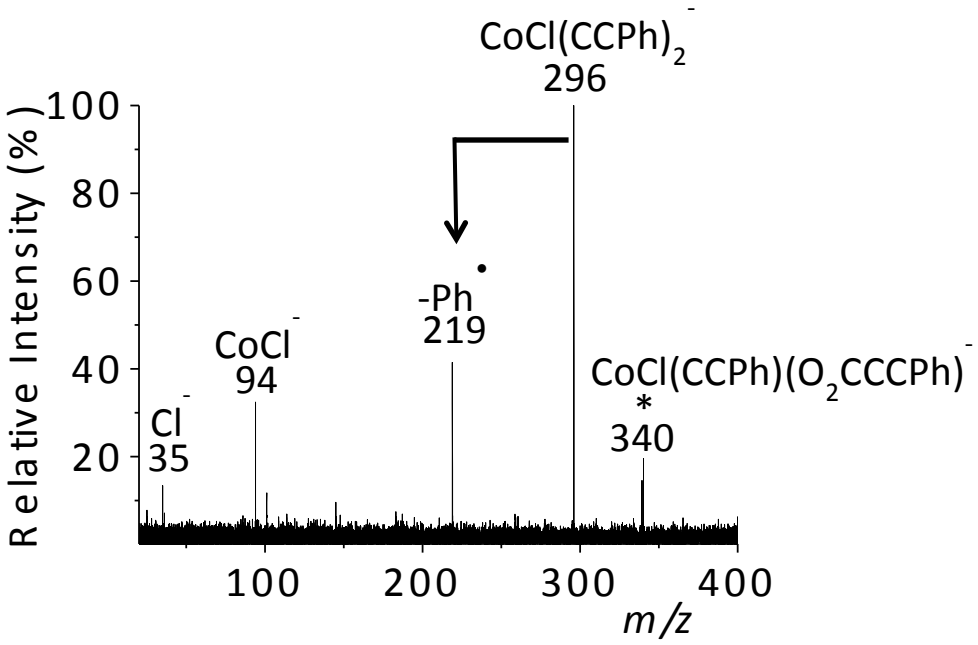

Figure S30: TOF mass spectrum of $CoCl(C{\equiv}CPh)_2^-$ (296 *m/z*).

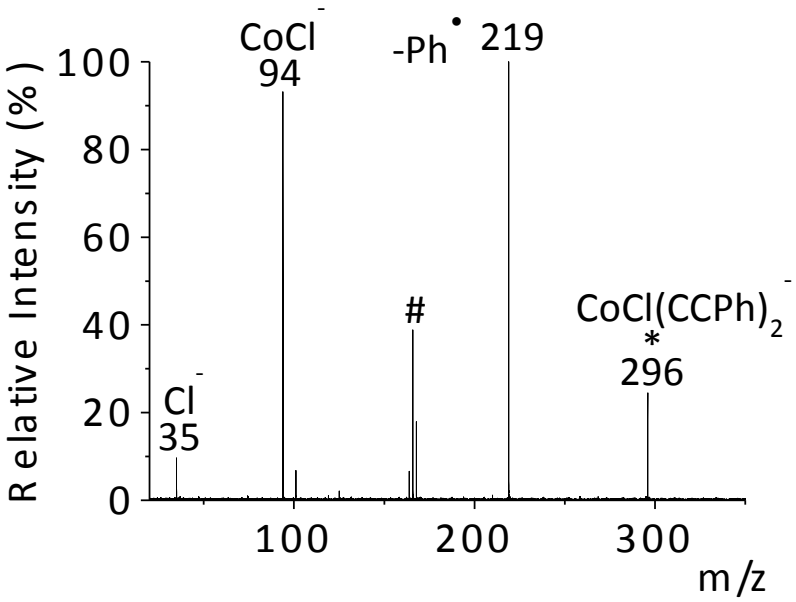

NB: Peak marked with # is assigned to the fragmentation product of an isobaric ion observed in the MS^1 spectrum

Figure S31: TOF mass spectrum of $CoCl(O_2CC{\equiv}CCH_3)_2^-$ (260 *m/z*).

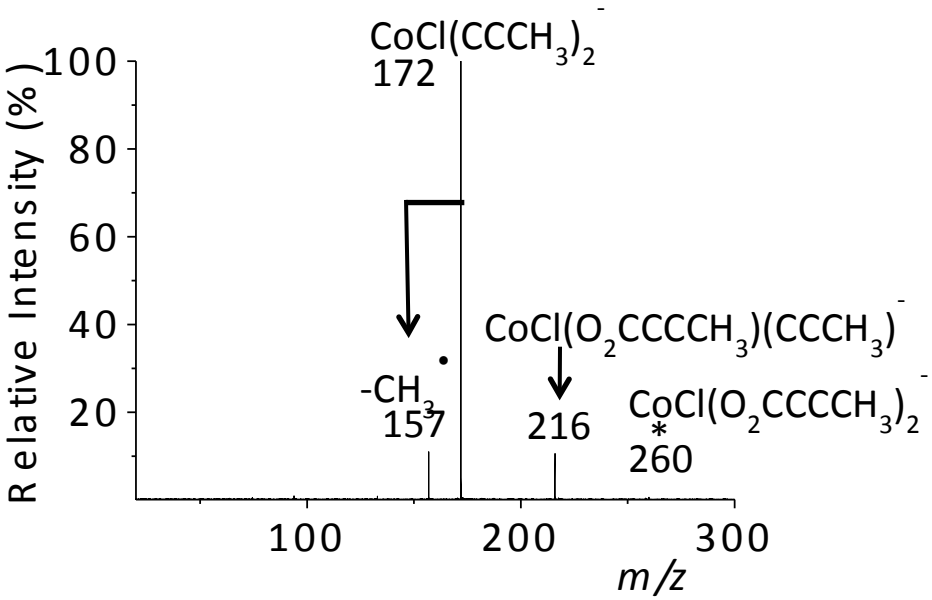

Figure S32: TOF mass spectrum of $CoCl(C{\equiv}CCH_3)(O_2CC{\equiv}CCH_3)^-$ (216 *m/z*).

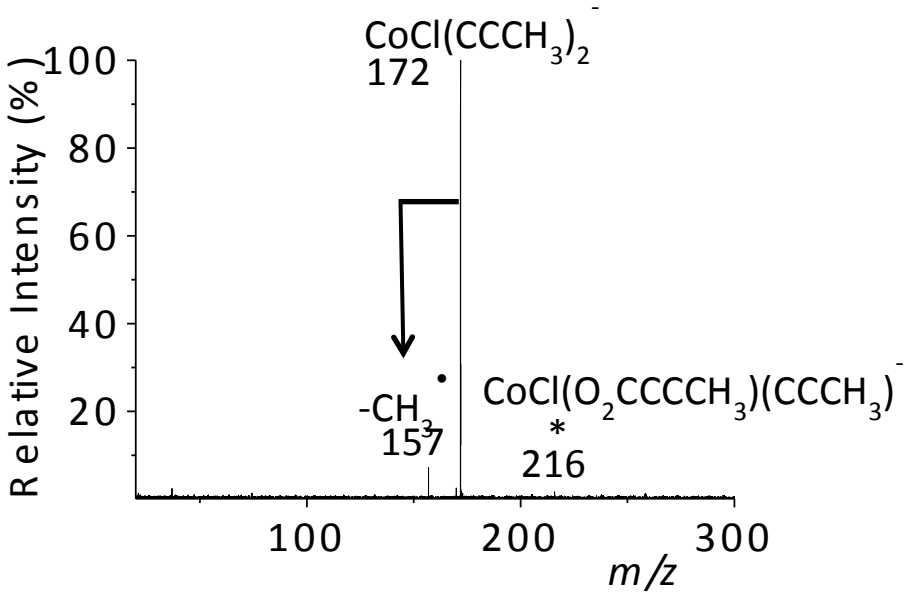

Figure S33: TOF mass spectrum of $CoCl(C{\equiv}CCH_3)_2^-$ (172 *m/z*).

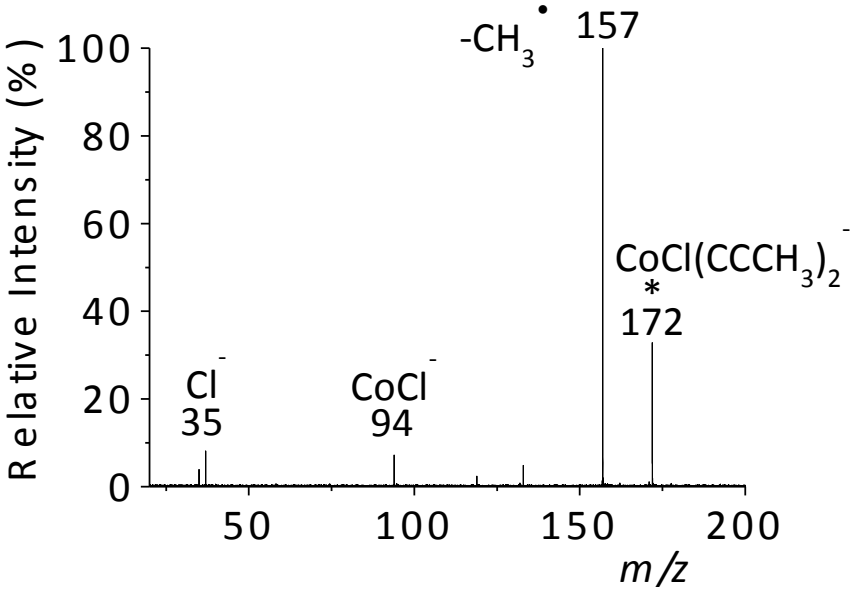

Figure S34: TOF mass spectrum of $CoCl(O_2CC{\equiv}CH)_2^-$ (232 *m/z*).

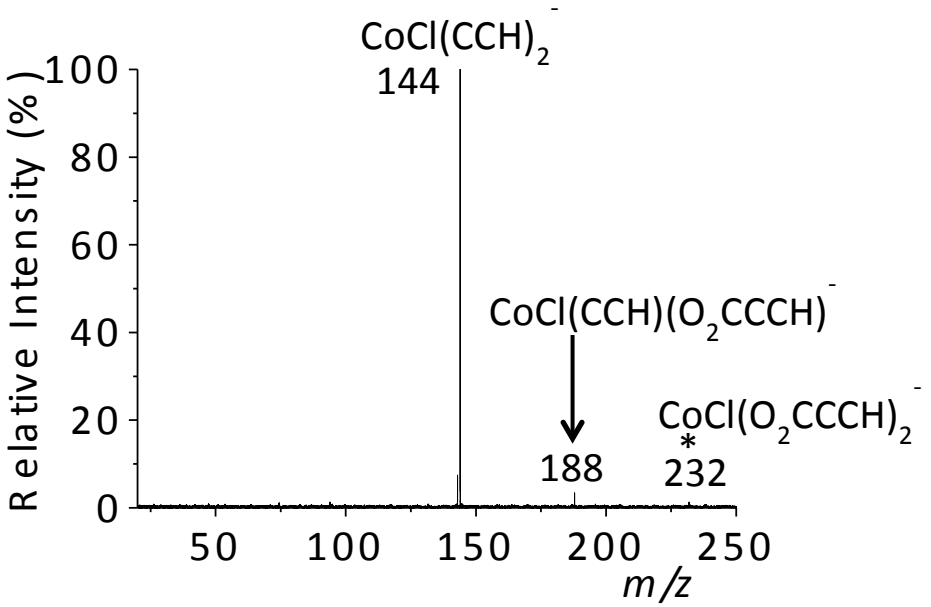

Figure S35: TOF mass spectrum of $CoCl(C{\equiv}CH)(O_2CC{\equiv}CH)^-$ (188 *m/z*).

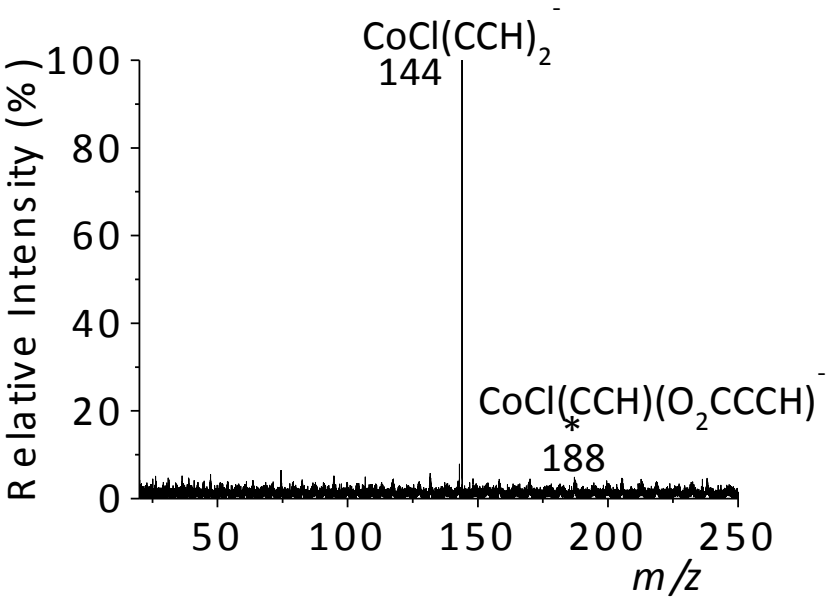
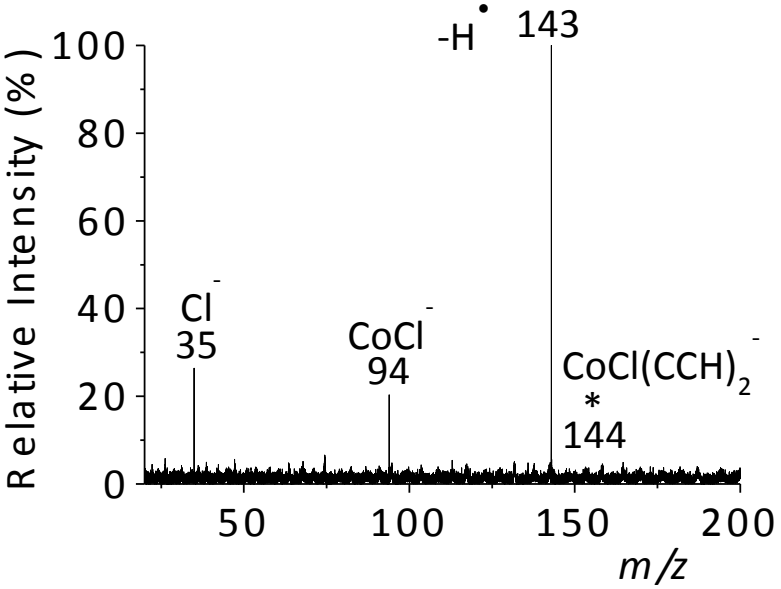
Figure S36: TOF mass spectrum of $CoCl(C{\equiv}CH)_2^-$ (*144 m/z*).